AGU100 ADVANCING EARTH AND SPACE SCIENCE

Water Resources Research

RESEARCH ARTICLE
10.1029/2018WR023190

Special Section:
Advances in remote sensing, measurement, and simulation of seasonal snow

Direct Insertion of NASA Airborne Snow Observatory-Derived Snow Depth Time Series Into the *iSnobal* Energy Balance Snow Model

Andrew R. Hedrick[1,2], Danny Marks[1], Scott Havens[1], Mark Robertson[1], Micah Johnson[1], Micah Sandusky[1], Hans-Peter Marshall[2,3], Patrick R. Kormos[4], Kat J. Bormann[5], and Thomas H. Painter[5]

[1]USDA-ARS Northwest Watershed Research Center, Boise, ID, USA, [2]Department of Geosciences, Boise State University, Boise, ID, USA, [3]U.S. Army Cold Regions Research and Engineering Laboratory, Hanover, NH, USA, [4]Colorado Basin River Forecast Center, National Weather Service, Salt Lake City, UT, USA, [5]Jet Propulsion Laboratory, California Institute of Technology, Pasadena, CA, USA

Abstract Accurately simulating the spatiotemporal distribution of mountain snow water equivalent improves estimates of available meltwater and benefits the water resource management community. In this paper we present the first integration of lidar-derived distributed snow depth data into a physics-based snow model using direct insertion. Over four winter seasons (2013–2016) the National Aeronautics and Space Administration/Jet Propulsion Laboratory (NASA/JPL) Airborne Snow Observatory (ASO) performed near-weekly lidar surveys throughout the snowmelt season to measure snow depth at high resolution over the Tuolumne River Basin above Hetch Hetchy Reservoir in the Sierra Nevada Mountains of California. The modeling component of the ASO program implements the *iSnobal* model to estimate snow density for converting measured depths to snow water equivalent and to provide temporally complete snow cover mass and thermal states between flights. Over the four years considered in this study, snow depths from 36 individual lidar flights were directly inserted into the model to provide updates of snow depth and distribution. Considering all updates to the model, the correlation between ASO depths and modeled depths with and without previous updates was on average r^2 = 0.899 (root-mean-square error = 12.5 cm) and r^2 = 0.162 (root-mean-square error = 41.5 cm), respectively. The precise definition of the snow depth distribution integrated with the *iSnobal* model demonstrates how the ASO program represents a new paradigm for the measurement and modeling of mountain snowpacks and reveals the potential benefits for managing water in the region.

Plain Language Summary In regions that depend primarily on snow to support life, water availability is becoming an increasingly important topic. National Aeronautics and Space Administration (NASA)'s Airborne Snow Observatory (ASO) is a new platform for estimating the amount of water stored in mountain snowpacks. Since 2013, the ASO has combined detailed measurements of snow depth from an aircraft with snowpack density estimates from a physics-based snow model to provide predictions of total snow water equivalent stored in the Tuolumne River Basin in the California Sierra Nevada. This work describes the process of updating the snow model using the measured ASO snow depths through a direct insertion process. When the distribution of all the snow in the basin is known more accurately, the model results are improved.

Key Points:
- This is the first near-real time application of a model state variable being periodically updated using lidar-derived snow depths
- The first update in each year is most crucial since it defines the spatial pattern of snow accumulation prior to peak snow water equivalent
- Ensuing updates remain important for setting the spatial distribution of spring storms and when the duration between flights is prolonged

Correspondence to:
A. R. Hedrick,
andrew.hedrick@ars.usda.gov

Citation:
Hedrick, A. R., Marks, D., Havens, S., Robertson, M., Johnson, M., Sandusky, M., et al. (2018). Direct insertion of NASA Airborne Snow Observatory-derived snow depth time series into the *iSnobal* energy balance snow model. *Water Resources Research*, *54*, 8045–8063. https://doi.org/10.1029/2018WR023190

Received 8 MAY 2018
Accepted 15 AUG 2018
Accepted article online 30 AUG 2018
Published online 19 OCT 2018

1. Introduction

In the western United States, mountain snowmelt is the primary source of water supply for domestic, agricultural, and ecosystem use; provides hydropower electricity to millions of people; and replenishes groundwater. In the state of California, the Sierra Nevada seasonal snowpack on average provides an additional 70% of water storage to the existing man-made reservoir system (Dettinger & Anderson, 2015). For most of the twentieth century, the relative stability of the relationship between point measurements of streamflow and snow water equivalent (SWE) at index sites allowed the use of empirical relationships for making decisions that affect downstream consumers and stakeholders, albeit with seasonal forecast errors of 20% to greater than 40% (Dozier, 2011). However, a warming climate shortens the duration of seasonal snow cover in the Northern Hemisphere, decreasing snowfall and subsequently the naturally stored water supply

(Derksen & Brown, 2012; Vaughan et al., 2013). With ever increasing demand, low precipitation totals, abnormally higher temperatures, and a reduced snowpack (Griffin & Anchukaitis, 2014; Henn et al., 2018; Margulis et al., 2016; Wilson et al., 2016), water supply forecasting is proving to be more important than ever before. The recent 2012–2015 California drought has reiterated the need to identify new methods to quantify water storage in mountain snowpacks.

Changes in the timing of snow cover accumulation and ablation alter the relationship between streamflow and SWE at index sites and drive the need for new approaches to better inform water resource management (Vano et al., 2012). To further complicate matters, snowpack mass (SWE) can change drastically over small distances in mountain basins because of the combined effects of highly variable wind fields, solar and thermal radiation, and topographic and vegetation structure (Anderton et al., 2004; Conway & Abrahamson, 1984; Grünewald et al., 2010). The timing of melt and delivery of water to the soil surface is never uniform, following high energy locations across the landscape as solar zenith angles and temperatures increase (Essery & Pomeroy, 2004; Luce et al., 1999). The physically based modeling and remote sensing assimilation approach presented here aims to address the source of greatest uncertainty for reservoir managers by more explicitly defining the quantity of water entering the mountain hydrologic system.

The National Aeronautics and Space Administration/Jet Propulsion Laboratory (NASA/JPL) Airborne Snow Observatory (ASO) launched during the winter of 2013 to provide distributed SWE and albedo estimates over large mountain basins. The ASO program provides more detailed estimates of basin snowpack storage for water managers and researchers through a unique coupling of multitemporal remote sensing and physically based snow modeling (Painter et al., 2016). To accomplish this, ASO performs airborne surveys every few weeks during accumulation and weekly intervals from peak SWE onward, deriving snow depths by differencing snow-free from snow-covered elevation surfaces obtained by its lidar scanner. The ASO-derived snow depth products are combined with *iSnobal* simulated snow density fields to produce 50-m spatial resolution daily images of SWE distribution and volume. *iSnobal* (Marks et al., 1999) is a distributed, physically based energy and mass balance snow model that explicitly solves for a number of snowpack properties including snow depth, density, and SWE.

Vögeli et al. (2016) demonstrated the value of redefining the spatial snow depth distribution of a physically based model using snow depths derived from a single lidar survey. Brauchli et al. (2017) took that approach a step further by demonstrating how streamflow responded to the more accurate snow distribution. Following those efforts, this paper describes how the ASO-derived snow depths were integrated into the *iSnobal* snow model in near real time over the Tuolumne Basin in the central Sierra Nevada for the first four years of the ASO program (2013–2016). This approach is providing water managers with periodic spot checks of how existing legacy models have been performing throughout the season and establishing the foundation for a new modeling paradigm.

2. Study Area

The Tuolumne River and its tributaries provide the fresh water supply for over 2 million people in the San Francisco Bay Area through a combination of winter snow storage in the upper elevations and careful water management of the system's reservoirs. The Tuolumne extends from just above the Central Valley floor to the Sierra crest and includes much of Yosemite National Park. Elevations within the 1,180 km^2 basin above the Hetch Hetchy Reservoir (Figure 1) range from 1,150–3,999 m above sea level, with slightly less than half of the basin below timberline. Tree line occurs at approximately 2,900 m, and the majority of the alpine terrain is composed of exposed granite bedrock. Historically, the lowest elevations (1,150–1,600 m, 4% of basin area) are rain-dominated where approximately 60% of the precipitation falls as rain. The region between 1,600–2,000 m (6% of basin area) is the rain-snow transition zone where most storms are a mix of rain and snow. The region above 2,000 m (90% of basin area) is snow-dominated where more than 70% of precipitation falls as snow (Lundquist et al., 2016). However, it is possible for rain to fall at the highest elevations of the basin and for snowfall to occur at the lowest. Two relatively small receding glaciers (Lyell and Maclure) are found in the southwest portion of the basin, but this work does not treat them separately from nonglaciated terrain.

Owing to the basin's location within the Yosemite National Park Wilderness Area, establishment and maintenance of weather monitoring stations is limited, and therefore, the measurement network used for the modeling work presented here is sparse (Figure 1). Additionally, scheduled routine site maintenance is

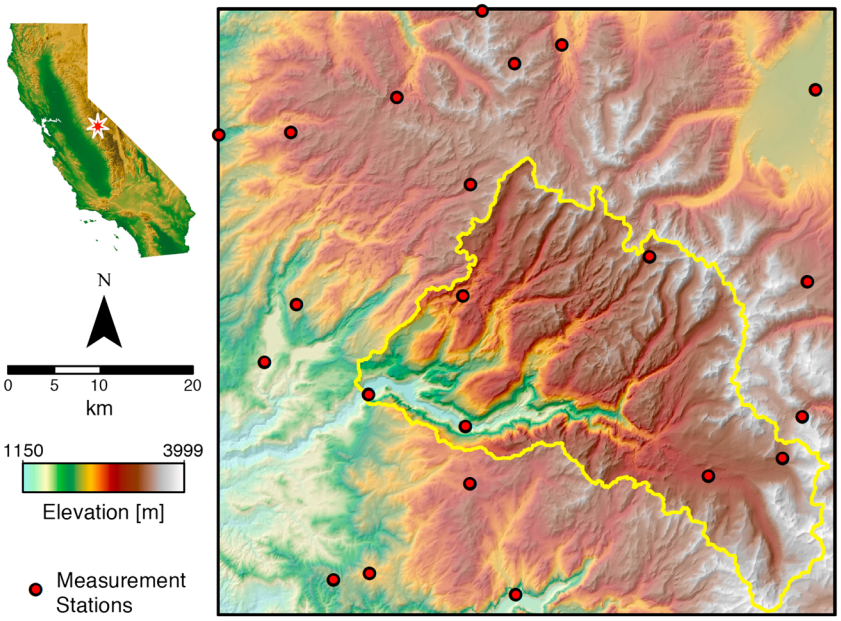

Figure 1. Location and relief map of the Tuolumne River Basin above Hetch Hetchy Reservoir within the U.S. State of California. Locations of various measurement stations used to force *iSnobal* in water year 2013 are depicted as red circles.

generally difficult or impossible since sites positioned in remote locations can only be accessed on foot or by horseback in the short summer snow-free season.

3. Background and Methodology

3.1. The Airborne Snow Observatory

Light detection and ranging (lidar) has been demonstrated to be an accurate tool for observing the spatial variability of snow depths in complex terrain (Deems et al., 2006, 2013; Prokop, 2008; Tinkham et al., 2014; Trujillo et al., 2007). ASO is the first operational campaign to use airborne lidar coupled with imaging spectrometry for hydrological forecasting applications (Painter et al., 2016). Its 24-hr turnaround time from the moment of aircraft landing to delivery of SWE products is crucial to the ASO mission objective due to the dynamic nature of the mountain snowpack.

Snow depths were measured by differencing a baseline snow-free surface from snow-on surfaces, obtained using ASO's Riegl Q1560 dual scanning lidar, combined with geographical analysis and constrained by classification from the visible-near-infrared spectrometer analysis and lidar return intensity (Painter et al., 2016). SWE, the primary concern for water managers and decision makers, can be estimated spatially from the product of the lidar-derived snow depths and modeled snow density fields. In its first two years, ASO planned to begin surveying at approximately peak SWE and continue flying weekly until complete melt out. As the ASO program began to characterize the dynamic nature of snow cover distribution, the decision was made to fly earlier to capture accumulation processes in the following years. This resulted in 6 surveys during the 2013 snow season (early April to early June), 9 surveys during the 2014 snow season (mid-March to early June), 9 surveys during the 2015 snow season (mid-February to early June), and 12 surveys during the near-average 2016 snow season (late March to early July; see Table 1).

Coincidentally, ASO captured the extreme California drought of 2012–2015, which brought the program to the attention of California water supply forecasters and stakeholders in a way that would not have

Table 1
Summary of Airborne Snow Observatory Surveys and Meteorological Measurement Stations, by Variable, Within the iSnobal Modeling Domain of the Tuolumne River Basin

		No. of available meteorological stations				
Year	No. of ASO updates	T_a	RH/e_a	u/u_{dir}	m_{pp}	S_{in}/cc_{frac}
2013	6	20	8	7	12	6
2014	9	23	10	7	15	5
2015	9	23	12	8	15	7
2016	12	21	10	7	14	7
	Interpolation Method	IDW	IDW	IDW	DK	IDW

Note. Available stations can vary and numbers presented correspond to maximum number of stations used over an entire water year. In addition, the specifics of the point measurement to regular grid interpolation for each variable are listed (T_a, air temperature; RH, relative humidity; e_a, vapor pressure; u, wind speed; u_{dir}, wind direction; m_{pp}, precipitation mass; S_{in}, incoming shortwave radiation; cc_{frac}, cloud cover fraction; IDW, inverse distance weighting, DK, detrended kriging).

been expected had these been typical or near-average snow years. Fortunately, the 2016 snow season was closer to the long-term average, so the analysis presented herein also includes a nondrought year.

3.2. *iSnobal*

The snow density modeling component of ASO was carried out over the winter/spring seasons concurrent with the airborne surveys (2013–2016). The initial task for the modeling component was only to provide distributed estimates of snow density in order to produce spatially distributed SWE products for downstream stakeholders, water managers, and forecasters. By the beginning of 2014 it became clear that the ASO program needed to more effectively integrate the *iSnobal* modeling components into developed products because users of the ASO products desired more than basin distributed and total SWE storage volumes. *iSnobal* is able to separate rain from snow while simultaneously providing detailed information on the distribution of SWE volume, snow cover thermal state, melt, and the delivery of melt-water or rain to the soil surface. However, due to the sparse meteorological network at higher elevations and the inherent spatial variability of mountain snow covers, the modeled snow distribution is consistently more uniform with less spatial variability than the distribution measured by the ASO surveys.

The ASO surveys provide periodic measurements of snow depth that define the true distribution of snow across large mountain basins. Additionally, *iSnobal* fills in the periods between ASO flights to provide a complete time series of snowpack evolution. We hypothesize that the integration of the ASO lidar-derived snow depth field into the *iSnobal* state variable data stream defines the true snow distribution and therefore improves the ability of the snow model to predict the energy and mass fluxes of the snowpack, similar to the findings of Brauchli et al. (2017) and Vögeli et al. (2016). Though touched on in this methodological study, future work will test this hypothesis in a more rigorous fashion.

In 2014, the USDA-ARS Northwest Watershed Research Center in Boise, Idaho, USA (henceforth the NWRC), began assimilating the ASO snow depth fields as a model state variable update to *iSnobal* in near real time. Figure 2 depicts the typical process for the initial model setup and the subsequent reinitializations when the ASO snow depth measurements become available. To the knowledge of the authors, this is the first near-real-time incorporation of high-resolution snow depths into the data stream of an energy balance snow model.

As a physically based, gridded snow model, *iSnobal* estimates snowpack properties given particular spatial and temporal meteorological forcing data (e.g., Marks et al., 1999). Designed to be computationally efficient while maintaining maximum portability, *iSnobal* explicitly solves the energy and mass balances at each grid cell over a digital elevation model grid, and therefore does not require site-specific calibration within the model itself. All meteorological forcing surfaces are assembled outside the model, and adjustments are performed at the user's discretion when producing the spatial forcings required by the model. The original *iSnobal* design concept was that the model should not make adjustments for limitations in available forcing data (Marks & Dozier, 1992). Instead of being built into the snow model, the methods used to develop the distributed forcing data surfaces are determined by any available weather station measurements, remote sensing data, or output from numerical weather models.

iSnobal was originally designed to accommodate periodic inputs from satellite or aircraft remote sensing data in the NASA Earth Observing System (EOS) era (Dozier, 1990). This design feature allows the model to be run forward to a time when model initialization or state data are available, stopped and updated, and then restarted. The ASO surveys provide unprecedented detail for the snow depth state variable, which can be reset midyear for a more accurate, updated estimate of snow distribution, resulting in improved model predictions.

Studies assessing *iSnobal* across a range of snow environments and snow-dominated basins are numerous in the literature. The temporal and spatial scales of various studies range from 0.015 km^2 over a 2.5-m grid (Kormos et al., 2014), 460 km^2 over a 75-m grid (Marks et al., 1999), 2,150 km^2 over a 250-m grid (Garen et al., 2001; Garen & Marks, 2005), 1,180 km^2 over a 50-m grid (this study), to 7,000-km^2 over a 100-m grid (Havens et al., 2016). Each of these assessment studies generated the required forcing parameter grids using different methods and at different spatial resolutions determined by available computational resources and study objectives. From the above referenced studies, the increase in computational resources over the last 15 years is evident. By streamlining source code and taking advantage of multiprocessor computing power, the recent

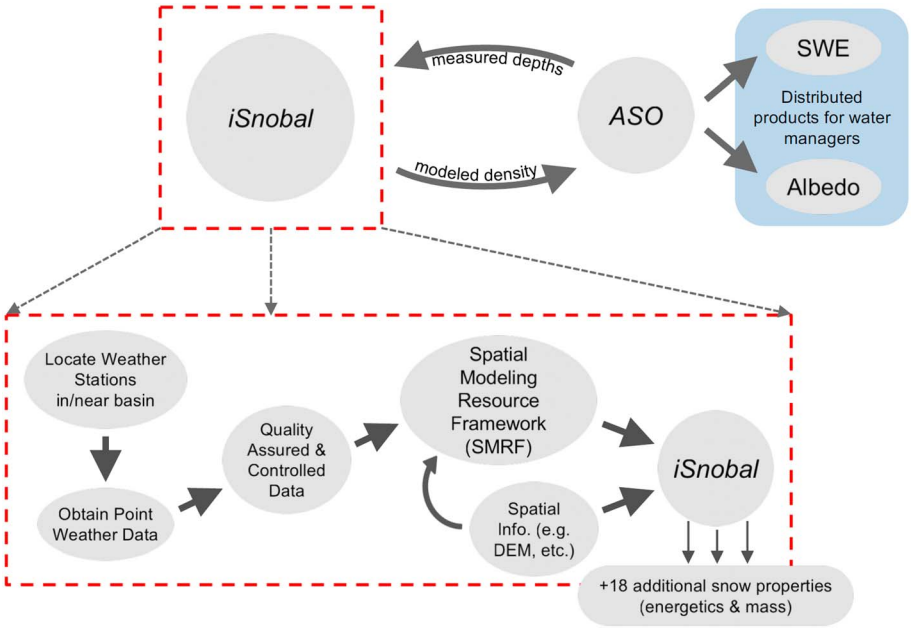

Figure 2. Exploded view of the workflow for the *iSnobal* modeling progression from initiation to delivery of model products to the ASO compute team. This chart includes the process of updating the *iSnobal* model state using the ASO lidar-derived snow depths.

upgrades to the modeling system represent a 200x increase in computational efficiency. This boost in efficiency allows the model to be run in near real time and errors in forcing data to be diagnosed in real time.

iSnobal can be implemented at any temporal resolution that can be supported by the available spatial forcings, though Garen and Marks (2005) point out that the selected temporal resolution must account for the diurnal cycle. In this work, hourly meteorological station measurements are the basis for the forcing grids and, accordingly, *iSnobal* is run at an hourly resolution onward from the onset of each water year (1 October). As input, *iSnobal* requires spatially gridded interpolants derived from point measurements of basic meteorological variables that are available from most standard mountain weather stations in the western United States (Table 1). In addition, indirect forcing grids of vapor pressure, net shortwave radiation, percent cloud cover, and incoming longwave radiation are computed through empirical relationships (described in section 3.2.1).

While *iSnobal* does not simulate belowground hydrologic processes or streamflow, it does explicitly deal with both rain and snowfall as input precipitation. Surface water input (SWI) is defined as either rain on bare ground or melt/rain that exceeds the liquid water holding capacity of the snowpack and drains through the snow to the ground surface. Percolation processes within the snowpack are not explicitly considered. The results presented here represent simulations for complete water years (1 October to the following 30 September), including both the wet and dry seasons.

3.2.1. Station Data

The six meteorological variables of air temperature (T_a), wind speed (u), and direction (u_{dir}), relative humidity (RH), incoming solar radiation (S_{in}), and accumulated precipitation (m_{pp}) are measured within or adjacent to the Tuolumne modeling domain at hourly temporal resolution (Figure 1). In California, weather stations are maintained by various cooperative agencies, and the data are collected and assembled by both the California Data Exchange Center (http://cdec.water.ca.gov) and MesoWest (Horel et al. (2002), mesowest.utah.edu/). Table 1 lists the number of stations that measured these six meteorological variables throughout each of the four years presented in this study. Since many stations occasionally went off-line at various times throughout the simulation years, the reported number of stations represents the maximum used throughout each complete water year. For instance, incoming solar radiation measurements were only available at four stations over the latter half of water year 2016. The quality of *iSnobal* model results are directly influenced by the quality of the point meteorological data used to create the spatial forcing grids. Additional in-house quality assurance and control is nontrivial and paramount for preparing the most accurate possible forcing data set over the model domain.

Table 2
iSnobal Input and Output Files

File	Variable	Description	Units
(a) Energy inputs (all time steps)	I_{lw}	incoming longwave radiation	W/m^2
	T_a	air temperature	°C
	e_a	vapor pressure	Pa
	u	wind speed	m/s
	T_g	soil temperature	°C
	S_n	net shortwave radiation	W/m^2
(b) Precipitation inputs (only during storms)	m_{pp}	total precipitation mass	mm
	P_{snow}	percent mass that fell as snow	0–1.0
	ρ_{ns}	new snow density	kg/m^3
	T_{pp}	average precipitation temperature	°C
(c) *iSnobal* outputs (previous time step)	z_s	predicted snow depth	m
	ρ	predicted average snow density	kg/m^3
	m_s	predicted specific mass of snow	mm
	h_2o	predicted liquid water in snow	mm
	T_{s0}	predicted active layer temperature	°C
	T_{sl}	predicted lower layer temperature	°C
	T_s	predicted average snow temperature	°C
	z_{sl}	predicted lower layer depth	m
	h_2o_{sat}	predicted liquid water saturation	%
(d) Restart/update initialization (state variables)	z	elevation	m
	z_0	roughness length	m
	z_s	ASO-updated snow depths	m
	ρ	average snow density	kg/m^3
	T_{s0}	active layer temperature	°C
	Tsl	lower layer temperature	°C
	Ts	average snow temperature	°C
	h_2o_{sat}	liquid water saturation	%

Note. (a) Hourly energy input forcing grids. (b) Hourly mass input forcing grids that are only required when precipitation is measured by one or more meteorological stations. (c) Output grids of snow mass and temperature from the time step prior to the Airborne Snow Observatory (ASO) snow depth update (energetics are written into a separate file not shown here). (d) Initialization grids for the iSnobal restart with the ASO update. Highlighted variables in (c) and (d) indicate parameters that must be spatially adjusted when incorporating the new snow depth measurements from the ASO.

Hourly measurements of all variables from every available station are automatically downloaded each day to a local database maintained at the NWRC. Manual and semiautomated quality assurance and control is performed on raw downloaded data to interpolate across small data gaps and remove spikes. Precipitation data are adjusted using the Automated Precipitation Correction Program (Nayak et al., 2008), which fills gaps and removes spikes using a bias-limiting noise reduction algorithm. The precipitation measurements are then adjusted for wind undercatch using standardized equations for either shielded or unshielded gauges according to Yang et al. (1998), depending on each individual sensor. All methods for dealing with raw station data are described in Havens et al. (2017). Agencies that manage stations in the western United States often report coordinates only to the tenth of a degree in latitude and longitude precision. Since accurate station locations are crucial for producing forcing grids at 50-m resolution over complex terrain, care has been taken to determine more precise coordinates.

In addition to the six available variables measured by automated weather stations, two additional point variables must first be calculated using those available measurements. Vapor pressure (e_a) is determined from the Clausius-Clapeyron empirical relationship at stations with measurements of air temperature and RH. Fractional cloud cover (cc_{frac}) is estimated from the ratio of measured incoming shortwave radiation to calculated clear-sky irradiance at locations where incident solar radiation is measured, similar to the method presented by Susong et al. (1999). A description of these data and the methods used in the creation of model forcing inputs is available in an accompanying data set (Hedrick et al., 2018a).

Table 2 details all of the generated snow properties and processes along with the energy and mass inputs and outputs for a typical model time step. The fundamental principles that *iSnobal* uses for calculating the snow cover energy and mass balance are based upon relatively straightforward and thoroughly validated

physical relationships. Therefore, when model estimates differ significantly from in situ measurements, then all adjustments and corrections must be performed on the forcing data provided to the model. Any necessary adjustment or correction to spatially distributed forcing data (e.g., estimated cloud cover, incoming thermal radiation, and the approximated precipitation distribution) must occur prior to model initialization. Poor or missing measurements may cause *iSnobal* to crash, so occasionally adjustments must be made to interpolate over a span of hours during a simulation cycle.

3.2.2. Spatial Forcing Grids

The Spatial Modeling Resource Framework (SMRF) is a tool for distributing various point measurements over a regular grid for near real-time applications (Havens et al., 2017). SMRF was developed in-house at the NWRC, and the latest stable release can be found at https://github.com/USDA-ARS-NWRC/smrf. The source code used for this study (SMRF v0.3.0) can be found within an open-source software repository (Hedrick et al., 2018b).

Various methods exist for distributing point measurements of meteorological variables over large areas and complex terrain (Garen et al., 1994; Goovaerts, 2000; Livneh et al., 2014; Luo et al., 2008). As a modular framework, SMRF permits the user to decide which method is appropriate for distributing each particular parameter. For instance, measured accumulated precipitation can be distributed in SMRF using either the detrended kriging (DK) or inverse distance weighting methodologies.

Table 1 summarizes the various distributing methods that were used throughout all four water years. The most suitable interpolation method depends on the meteorological variable being distributed. For instance, precipitation during storms is often spatially inconsistent over large mountain basins and generally exhibits a positive local elevation gradient (Lundquist et al., 2010). On the other hand, temperature typically displays a negative elevation lapse rate and is spatially continuous. These two variables require gridded interpolation methods that are appropriate for representing the differing physical processes at work.

Forcing grids were constructed at a 50-m spatial and hourly temporal resolution. In mountain basins it has been shown that the typical length scale of hydrologic variability is between 50 and 100 m (Deems et al., 2006; Pomeroy et al., 2006; Shook & Gray, 1996; Trujillo et al., 2007; Winstral & Marks, 2014), particularly for wind-exposed terrain where snow redistribution dominates the snowpack spatial variability. Therefore, at 50-m resolution, the model is expected to explicitly capture many of the physical processes that control the spatial distribution of the snowpack.

A crucial energy input to *iSnobal* is net shortwave radiation (S_n), which is the difference between incoming (S_{in}) and outgoing (S_{out}) solar radiation. S_n is seldom measured, but S_{in} is more often available. To estimate S_{out}, snow albedo (α) is simulated based on the elapsed time since the last snowfall for each model pixel and an assumed dust or debris content (Marks & Dozier, 1992; Marshall & Warren, 1987). Parameterizing surface albedo has been found to be difficult in mountainous regions (Guan et al., 2013; Molotch et al., 2004). Since accurate in situ measurements of snow albedo are only available at a few sites in the western United States, spatially distributed estimates of surface reflectance add a significant source of uncertainty into the model forcings. ASO is able to produce an albedo product from the onboard spectrometer, and ongoing research is investigating the nontrivial problem of assimilating the ASO albedo product into the model data stream. Since α is used to derive S_n for each time step, it is not a state variable of *iSnobal*.

Clear-sky, terrain corrected solar radiation is computed from Dozier (1980) and Essery and Marks (2007) using the ASO 50-m snow-free digital elevation model grid. Canopy shading is computed from the National Land Cover Database using methods described by Link et al. (2004) and Essery et al. (2008). Incoming longwave radiation (I_{LW}) is rarely measured so it is modeled from a combination of empirical relationships of clear-sky emissivity adjusted for terrain from Marks and Dozier (1979), and vegetation canopy cover and estimated cloud cover from available S_{in} measurements similar to Link and Marks (1999) and Reba et al. (2011). Wind speeds are distributed using the maximum upwind slope terrain parameter, S_x (Winstral et al., 2002), and methods described by Winstral et al. (2009). The calculations of energy transfer between the snow surface and the atmosphere used a surface roughness length of 1 mm for cells below the canopy and 5 mm in forest openings and above tree line.

For this modeling exercise soil temperatures (T_g) were set to a uniform −2.5 °C at a depth of 10 cm below the snow-soil interface, which is cold enough to allow the initiation of the snowpack but not so cold as to retain

snow on the ground late in the ablation season. Bair et al. (2018) showed that the ground temperatures at the nearby Mammoth Mountain CUES study plot fluctuated around −0.5 °C throughout the winter. Future studies will examine the impact of spatially and temporally representative soil temperature approximations.

Precipitation is by far the most critical input parameter for any snow or hydrologic model. Prior to model execution and through empirical relationships with the average precipitation temperature (T_{pp}—approximated by the distributed dew point temperature), precipitation mass (m_{pp}) is parsed into percent snow versus rain (P_{snow}), while the density of new fallen snow (ρ_{ns}) is calculated on an individual storm basis. Storm snow densification is computed similar to Table 1 in Marks et al. (1999) but is augmented in this work to consider compaction effects during storms from the changing overburden pressure. Before, during, and after the ASO snow depth acquisitions, the precipitation distribution and phase are approximated based on the limited number of precipitation measurement sites in and around the modeling domain. For these stations we estimate the elevation trend and distribute the undercatch-adjusted precipitation volume and phase across the modeling domain. A storm event is defined spatially and can extend either over all or a localized subset of the modeling domain. Within an event region, precipitation phase varies according to dew point temperature, so each storm event can be spatially subdivided into rain, mixed phase, and snow pixels for each storm hour. A more rigorous description of the computations involved for all spatial forcing fields—both energetics and mass—is detailed in Havens et al. (2017).

The primary objective of *iSnobal* in the context of ASO is to produce spatial snow density estimates. The mechanisms within a snowpack that influence bulk density are energy fluxes due to temperature gradients, liquid water content, compaction due to overburden, and time since accumulation (Kojima, 1967). Previous versions of *iSnobal* simply generalized the effects of temperature and overburden compaction into an empirical formulation dependent only upon time. Recent modifications to the model now permit distinct consideration of bulk compaction and temperature metamorphism. These modifications were included in the model results presented in this work.

3.3. Modeling and Direct Insertion

Each year during the accumulation period (typically October–February), the process of preparing data for running *iSnobal* begins with a thorough analysis of available meteorological station data in order to update the meteorological database with any stations that may have come online or malfunctioned. After constructing the spatial forcing grids described in section 3.2.2, *iSnobal* is then executed from the previous 1 October, the beginning of the water year, up to the date of the first ASO flight.

ASO derives gridded estimates of SWE by multiplying the lidar-derived snow depths and the snow density estimates given by *iSnobal* (Painter et al., 2016). This study focuses on the methods for assimilating the measured ASO snow depths into *iSnobal* and the effects of this integration on subsequent model results. Vögeli et al. (2016) and Brauchli et al. (2017) demonstrated the value of redefining the spatial snow depth distribution for input to a physically based model using remote sensing information. Over the four water years presented here, a modified direct insertion technique was developed to create the functional initialization files required to restart *iSnobal* after each survey (Table 2d). We refer to the method as "modified" because additional model state variables besides snow depth must be adapted to match the spatial extent and depth of the snow cover measured by the ASO lidar surveys.

Four scenarios are possible when modeled snow depths from the previous day are discarded in favor of the lidar-derived measurements. The first case is trivial, in which both the ASO and the model agree that a cell is snow-free so no change is made to the model states. The second scenario occurs when both the model and the ASO agree that a cell is snow-covered but disagrees on the height of the snow. In this case, the ASO snow depth is inserted into the model, and the remaining state variables (density, layer temperature, and liquid water content) are unchanged. A third case is when *iSnobal* predicts a snow cover, whereas the ASO measures a snow-free grid cell. When such discrepancy occurs, all other state variables are changed to represent a grid cell with no snow. On the other hand, it can be the case that the ASO measures snow and *iSnobal* has estimated the cell to be snow-free. In this fourth scenario, the snow density, layer temperatures, and liquid water saturation must be interpolated to match the perceived ASO snow cover.

To create reasonable values for each of the state variables that are required to restart *iSnobal*—those highlighted in Table 2d—an expanding window is applied where a minimum of 10 nearby snow-covered cells

must be found before averaging and moving on to the next cell. For these cells, the interpolated values are used for the new initialization of the model (Table 2c, following time step) so that cells with lidar-derived snow also contain estimates of bulk density, layer temperature, and liquid water content. In this way we resolve fringe effects from the discrepancies between model results and the remote sensing product in areas of patchy snow cover. Even so, the vast majority of these discrepancies in spatial extent occur within low elevation pixels that contain very little snow and therefore have a minimal effect on the total basin water storage.

4. Results

Over the course of the 2012–2015 drought, snowfall in the Tuolumne Basin was substantially lower than average. The 2015 snowpack, in particular, was the lowest in recorded history and determined to have the lowest April 1 SWE in over 500 years through tree ring peak SWE reconstruction (Belmecheri et al., 2016). Water year 2016 provided some relief from the drought with a snowpack that was ~85% of average. Some basic modeled hydrologic conditions derived by *iSnobal* during the study period (2013–2016) are presented in Table 3. These metrics were derived from the preprocessed precipitation forcing grids used as *iSnobal* input and described in section 3.3. The average rain-snow transition elevation was determined by finding the hourly median elevation of the pixels that were designated as mixed phase during each storm and computing a mass-weighted average over the water year.

The distribution of mountain SWE accumulation and ablation is governed by elevation gradients, vegetation, aspect, and slope. To investigate the impact of the ASO updates on the model, three elevation bands of the lowest 40%, middle 40–70%, and upper 30% of the basin area were delineated from the *iSnobal* results for 2013 to 2016 (Figure 3). The first ASO update adds SWE in the upper 30% of the basin in each of the four years, possibly due to precipitation measurement stations at higher elevations exhibiting greater undercatch than those at lower elevations (Rasmussen et al., 2012). At the same time, the ASO updates throughout the ablation season cause *iSnobal* to melt the snowpack earlier for elevations below 2,900 m. Also, it is apparent that the lower 40% of the basin was rain-dominated in 2013–2015 since the cumulative SWI curve is greater than the SWE curve throughout each full water year. The average water year (2016) received a more substantial snowpack at lower elevations. Above 2,700 m, which comprises 60% of the land area within the basin, snow storage dominated the system in all four years for the primary accumulation period of December through April.

In order to more specifically detail the spatial effects of the ASO updates, two individual updates were chosen from 2014 and 2015 that portrayed a large dynamic range in the basin-averaged change in water storage (ΔSWE; Figure 4). The 23 March 2014 update represented the largest positive ΔSWE (+40.8 mm) from any of the 36 updates applied over the study period, whereas the 1 May 2015 update had a much smaller effect on the basin-averaged ΔSWE ($-$7.1 mm). To delve into the qualitative change in spatial distribution from the ASO updates, Figure 4 shows the SWE from *iSnobal* alone, *iSnobal* with the ASO snow depth update, and ΔSWE over the entire basin for the same two updates. Insets show the fine scale changes in SWE distribution due to the snow depth update. Moreover, elevation lapse rates play a large role in the DK algorithm for distributing precipitation. For that reason, more refined equal area elevation bands were constructed to further assess how ΔSWE from the ASO updates were distributed across elevations (Figure 5). For the first update of 2014, the majority of the change was in the form of a net gain over the upper 50% of the basin (bands 6–10). On the other hand, the 1 May update spreads the difference across the middle elevations with negative changes in bands 3 to 8 and negligible change in the lower 20% and a slight increase in SWE over the upper 20% of the basin. Within some bands in Figure 5 the mean ΔSWE is not within the interquartile range meaning that outliers are skewing the distribution. This occurs generally at lower elevations where the sample size of pixels containing snow is relatively small and the influence of outliers is more considerable.

A linear regression analysis was performed between the ASO-derived snow depths from each flight and both the previously updated (for the second survey onwards) and the ordinary nonupdated *iSnobal* control runs. For each grid cell, the previously updated *iSnobal* snow depth estimates were highly correlated with the new depths from the subsequent ASO updates. However, the control run did not benefit from the previously redefined depth distribution and was poorly correlated to the lidar distribution.

Table 3
Hydrologic Metrics Derived From the iSnobal Precipitation Forcing Grids and ASO-Updated SWE Estimates

Year	Snow proportion of annual precipitation (%)	Average rain-snow transition elevation (m)	Date of peak SWE	Mean peak SWE (mm)
2013	83.0	2,016	11 March	323
2014	81.8	1,918	6 April	253
2015	71.3	2,394	10 February	124
2016	83.9	1,828	22 March	557

Note. Precipitation phase was determined using the distributed dew point temperature for every hour of each storm.

Figure 6 shows the scatter plot of all grid cells within the basin along with the fitted linear regressions for the seventh seasonal survey of 2015 on 1 May and the same update portrayed in Figures 4 and 5. Up to that point in 2015 the modeled snow depths never surpassed 1.5 m, but ASO measure depths as high as 4 m in a handful of pixels. At the same time, from the slope of the regression line for the previously nonupdated *iSnobal* results (red line) it is apparent that a large portion of cells saw a decrease in depth from the update. Performing the same analysis on all updates over the four-year study period clearly shows the influence of setting the snowpack spatial distribution with the first update of each year (Figure 7). This result is unsurprising since the DK method for distributing precipitation resolves the elevational gradient, yet does not account for aspect, slope, and vegetation, which are the most important controls on local scale variability. Also, evident is that the r^2 decreases occasionally throughout each year for even the updated model. We found this to be caused by two likely factors. First, late season storms that occurred between ASO surveys deposited snow preferentially, which was not accounted for by the DK precipitation distribution. Second, the time duration between subsequent surveys caused the model to drift further from the realistic distribution through uncertainties in the energy balance. For the majority of the ASO survey dates, the r^2 remained above 0.9

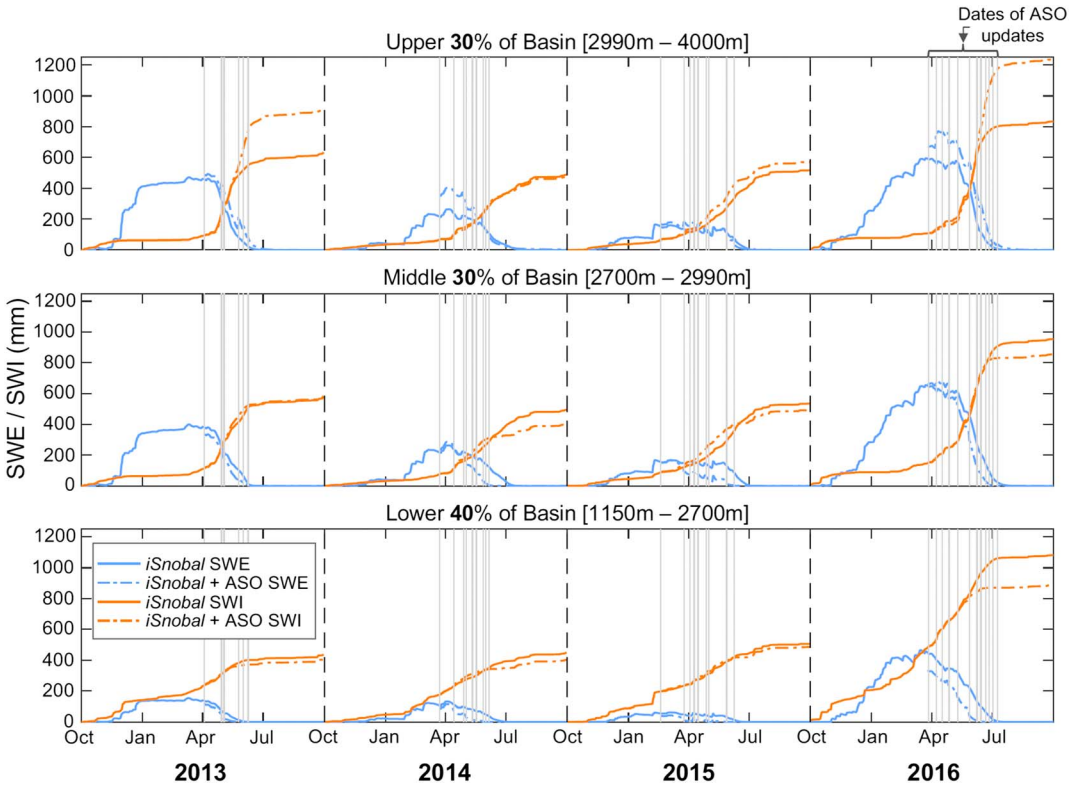

Figure 3. Basin-averaged *iSnobal* snow water equivalent (SWE) and surface water input (SWI) over three elevation bands for both the unmodified and ASO-updated predictions. The three bands, delineated by area, reveal elevations most sensitive to direct insertion of the lidar-derived snow depths. From the initial ASO update SWE is added at upper elevations for all four years, while complete melt out occurs earlier at middle to lower elevations.

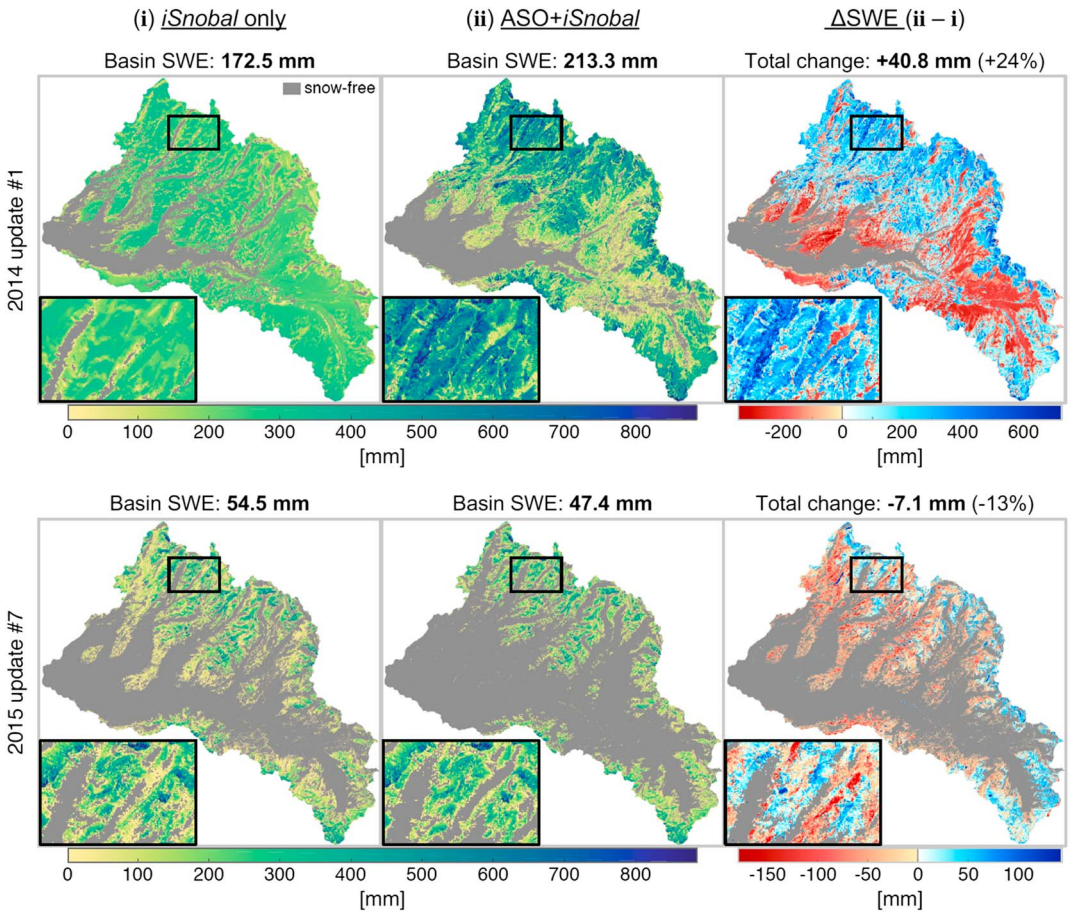

Figure 4. Spatial iSnobal SWE distribution both without the lidar update (i) and with the update (ii) applied for two surveys from water years 2014 and 2015, and the change in SWE resulting from the direct insertion of snow depths into the model. Inset areas (5.0 by 7.5 km) reveal the enhanced detail of the change in modeled SWE distribution from the ASO updates. The spatial distribution is most refined for the first update of the year (update #1, top row) and results in a much larger change in SWE than the updates later in the ablation season (update #2, bottom row), which benefit from prior snow depth updates. Updates correspond to those also shown in Figure 5.

throughout the melt, indicating that *iSnobal* performs best when provided with a spatially representative snow depth distribution. The mean coefficient of determination when considering all 32 updates that had a previous update earlier in the season was $r^2 = 0.889$ with a mean root-mean-square error of 12.5 cm. This is a much higher correlation than for those snow depth distributions that did not benefit from previous ASO updates ($r^2 = 0.162$, root-mean-square error = 41.5 cm).

The full basin-averaged *iSnobal* simulation results are depicted in Figure 8. The timings of the ASO lidar surveys are indicated, and simulation results are shown with and without the lidar-derived snow depth updates. In contrast with the elevation-resolved SWE, differences in total basin results between *iSnobal* estimates with and without the benefit of the ASO lidar updates are generally not large, but as shown previously they are initially spatially erroneous. In other words, the amount of solid precipitation input to the basin agrees with the ASO measurements, but the spatial distribution used to force the model is more uniform and does not account for drift and scour zones. Also shown are the SWI differences before and after adjustment. As mentioned before, SWI includes both snowmelt and rain and represents liquid water input to the soil. Changes in year-end SWI magnitude are relatively small in all years, with an increase of 14% in 2013, 2014, and 2015 decreasing 10 and 1%, respectively, and 2016 gaining only around 1%.

As a result of the ASO depth updates, the timing of the SWI shifted earlier in 2015 by a few weeks between mid-March and mid-June. Similarly, modeled SWI shifted slightly earlier in 2014, but the shift occurred later in the season and only for the month of May. In 2013 and 2016, the SWI pulse was largely unchanged in timing

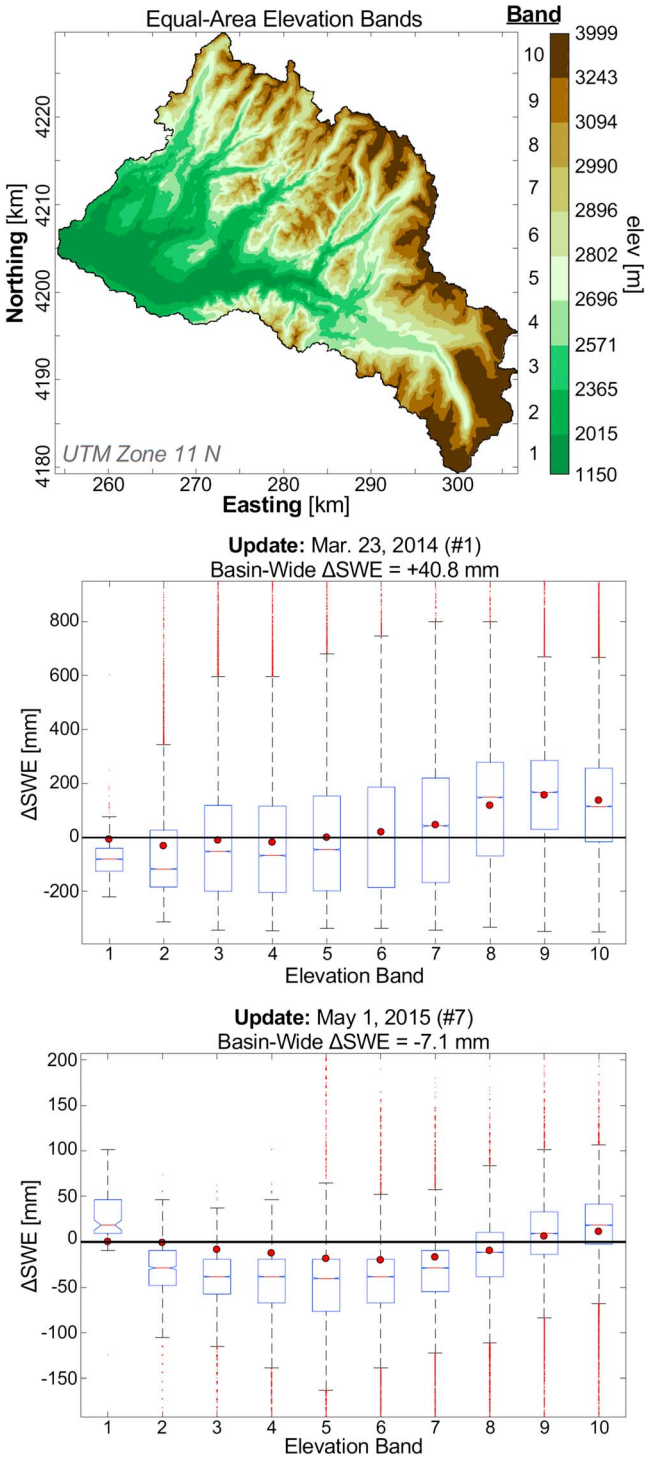

Figure 5. *iSnobal* change in SWE from two ASO updates delineated by equal-area elevation bands. Each band (area ≈ 118 km^2) makes up 10% of the total basin area. The y-axis of the box plot is the total change in basin SWE resulting from the update, while the elevation bands depicted at top are on the x-axis. Red circles show the mean ΔSWE contribution per band, while box plots display ΔSWE distributions within bands. Note the significant scale difference on the box plot vertical axes.

with the addition of the ASO updates. However, in 2013 the cumulative SWI increased by approximately 80 mm due to the addition of mass from the last three updates. The SWE and SWI curves for 2016 in Figure 8 display reflective symmetry throughout the ablation season since very little spring or summer rain occurred. In 2014 and 2015 substantial spring and summer rain took place after the basin SWE was depleted by the end of June.

5. Discussion

The first operational season of the ASO (water year 2013) happened to be the second year in what would eventually become a severe four-year drought. Not only was precipitation scarce over the Sierra Nevada, but temperature during storms was also above average resulting in reduced snowfall cold content. The ASO mission was serendipitously timed to facilitate water cycle science and aid water managers in their efforts to maintain reservoir levels during the California drought. The purpose of the analysis presented here was to show the influence from periodically redefining the spatial distribution of snow depth for a physically based snowmelt model. Over all four years, the general net impact of the updates was to initially increase SWE in the upper elevations from the first few updates and subsequently reduce SWE and melt the snowpack earlier in the middle to lower elevations as the ablation season progressed (Figure 3). There are likely several reasons for this behavior, but we believe two factors to be the primary causes.

First, during the winter accumulation period the distribution of precipitation mass from point measurements to a regular grid partially resolved the snowfall elevation gradient but was independent of local terrain and vegetation features. The resulting distribution lacks snow drifts and scour zones, important features of mountain snowpacks that influence storm snow density. The resulting energy budget would add uncertainty to estimates of early season melt before the first ASO survey. Additionally, correspondence with Hetch Hetchy Reservoir managers revealed that the actual precipitation undercatch for many of the gauges in and adjacent to the Tuolumne Basin was larger than accounted for in our applied undercatch correction. Rigorous future testing of these sites should evaluate this local knowledge and justify adjusting the precipitation forcing estimates in addition to the gauge undercatch corrections currently being used. Obvious elevational biases were introduced by the precipitation distributing technique used in the preprocessing steps to run *iSnobal* (Figures 3–5). The DK technique effectively reduces bias in the distribution only when point measurements are unbiased themselves. This is because the DK algorithm forces grid cells containing measurement stations to retain those values after the interpolation has been fit. However, the undercatch bias of low elevation measurement sites causes the slope of the precipitation elevational gradient to be reduced.

Second, the acceleration of the spring melt evident from the late season ASO updates could be a result of a lack of proper parameterization of net all-wave radiation. Thermal radiation is altered due to increased sensible heat in areas of patchy snow covers because of advection from exposed rock and soil (Olyphant & Isard, 1988; Pomeroy & Brun, 2001), which the ASO data are able to capture and *iSnobal* does not specifically account for. Without ASO depth updates, the modeled snow cover is

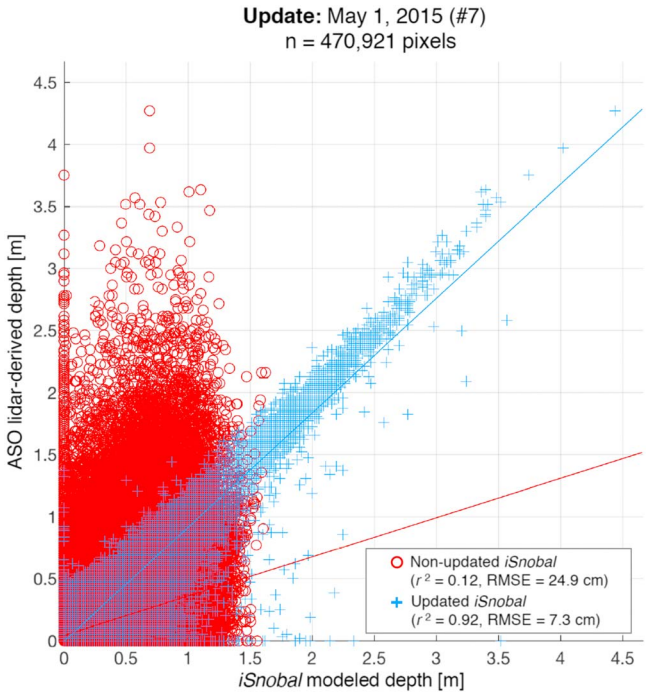

Figure 6. Scatter plot of ASO snow depths and both *iSnobal* snow depths with and without prior ASO updates for the seventh update of the 2015 water year. With previous updates, the spatial distribution is accurately defined and model estimates are highly statistically correlated to the ASO-derived snow depths.

more uniform and the model is unable to account for this increase in energy. Furthermore, net shortwave radiation input to *iSnobal* is a function of gridded spectral albedo, which is calculated from an empirical relationship (Marshall & Warren, 1987) and adjusted for litter accumulation on the snow surface (Hardy et al., 2004). The albedo decay function used here could lead to a miscalculation of net solar radiation, but we are not able to speculate whether modeled albedo is too high or too low, given that albedo is not measured in the basin. In water years 2013 and 2016 the model melted snow faster than ASO (individual updates added SWE late in the season) and in 2014 melted slower (updates removed SWE). Water year 2015 had no discernable trend in the updates themselves, but the updated modeled SWE melted much faster than the case without updates. Future work using the ASO-derived vegetation information and spectral albedo measurements could lead to a new parameterization and more accurate melt timing.

The ASO flights quantify the structure of the spatial distribution of the snowpack, thereby reducing the uncertainty introduced by the more uniform precipitation distribution (Table 2b) determined through DK. Figure 4 depicts the SWE distributions both before and after two updates in water years 2014 and 2015, along with the ΔSWE produced by each update. The first update of 2014 added a substantial amount of SWE to the basin, while the seventh update of 2015 had a much smaller effect on the storage. This demonstrates that by the time of the seventh update, the spatial variability of the snowpack was already captured by the previous six ASO acquisitions and the uncertainty due to the preprocessing step of distributing precipitation from point measurements was reduced considerably. Earlier ASO acquisitions in the accumulation season would also be able to characterize the actual distribution of individual snowfall events replacing the more uniform DK point to grid distribution, though this would be challenging due to the rapid densification of new snow and sensitivity to estimated new snow density. However, it is clear that regular updates reduce divergence in simulated SWE distributions when large storms occur across the basin.

Examining the modeled spatial distribution of snow depths over time with respect to each ASO-derived distribution verifies that the snow depth updates improve model performance. The modeled depths shown in Figure 6 are highly correlated to the ASO depths only when previous updates have redefined the spatial distribution. This redefinition of the snowpack distribution alters the model energetics and the resulting modeled SWI to the soil interface. The high correlations for the previously updated *iSnobal* estimates to the ASO depths continues throughout the year (Figure 7), indicating that the spatial extent of the updated model depths tend to be consistent with the ASO measured snow depths through the final survey of each year. However, the r^2 drops markedly to ~0.8 for flights that occurred either after large storms or after greater than three weeks had passed since the prior update. For instance, snowfall events occurred in May for both 2014 and 2015, and a dip in the correlation coefficient can be seen with the updated depths for those years in Figure 7. While *iSnobal* without updates accurately simulates total basin SWE magnitude, this indicates that ASO snow depths are critical for correcting the spatial pattern of snow accumulation. In contrast, *iSnobal* models melt quite well in the absence of late season storms.

Direct insertion data assimilation (DA) is not usually considered to be a robust technique since model fidelity is sacrificed and error in the assimilated measurement is ignored. A firm understanding of the relative model and lidar uncertainty must be known in order to employ other DA methods such as variational ensemble filter techniques (Auvinen et al., 2010; Houser et al., 2012; Miller et al., 1994). Running *iSnobal* in a near-real-time prediction setting along with computational constraints makes it currently impossible to perform robust error analysis using typical ensemble or Monte Carlo methods. Furthermore, studies are numerous in the literature that use point measurements to evaluate gridded model predictions. Though meteorological measurements from cooperator stations and the SNOTEL network were

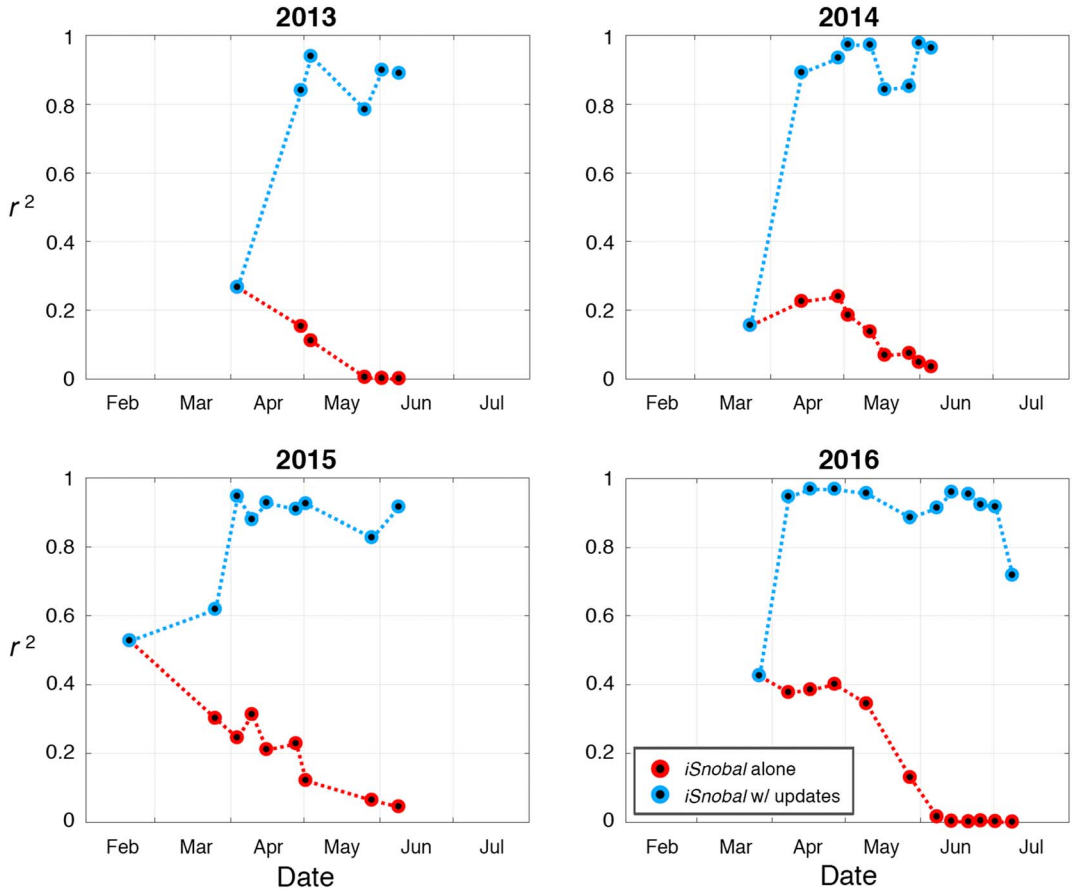

Figure 7. Coefficients of determination for each of the ASO-derived snow depth products with respect to *iSnobal* predicted snow depths on the day of the lidar acquisitions for both the previously updated (blue) and ordinary estimates without ASO (red). Once the spatial distribution is defined by the first update, the correlation to subsequent updates drastically increases.

designed to collect data that most closely represents the local physiography, they have been shown to be biased toward more sheltered sites and can be unrepresentative of the average conditions over an entire grid cell (Molotch & Bales, 2005).

The ASO lidar measurements, typical of any remote sensing platform, include a certain amount of uncertainty. Previous studies estimated uncertainties of lidar-derived snow depths between 15 and 30 cm using in situ measurement transects (Deems & Painter, 2006; Tinkham et al., 2014), but these studies were hampered by older lidar technology and Global Positioning System coregistration errors. Systematic errors can be introduced by Global Positioning System timing, the inertial measurement unit, or in postprocessing procedures. However, the snow depth product at the 3-m grid resolution possesses less accuracy across the study area than the 50-m product used for *iSnobal* direct insertion. For instance, the uncertainty in snow depth for the 3-m ASO snow depth product is ±8 cm (16 cm root-mean-square deviation; Painter et al., 2016). For that same survey flight, the average uncertainty over a 50-m pixel (made up of ~278 3-m cells) is approximately ±0.5 cm under the assumption of limited bias within the 50- by 50-m area of each grid cell.

Nevertheless, the major assumption being made in order to use the direct insertion DA method is that the lidar-derived snow depths are the truth and all uncertainty stems from the modeled SWE estimates when density is unchanged. Deeper snowpacks exhibit higher densities from compaction due to overburden (Sturm et al., 2010), so *iSnobal*'s density algorithm was reformulated to address this process. The model densifies pixels that receive any additional snow from the ASO update over the course of the next few model time steps. However, an example of the limitations of direct insertion DA is evident for water

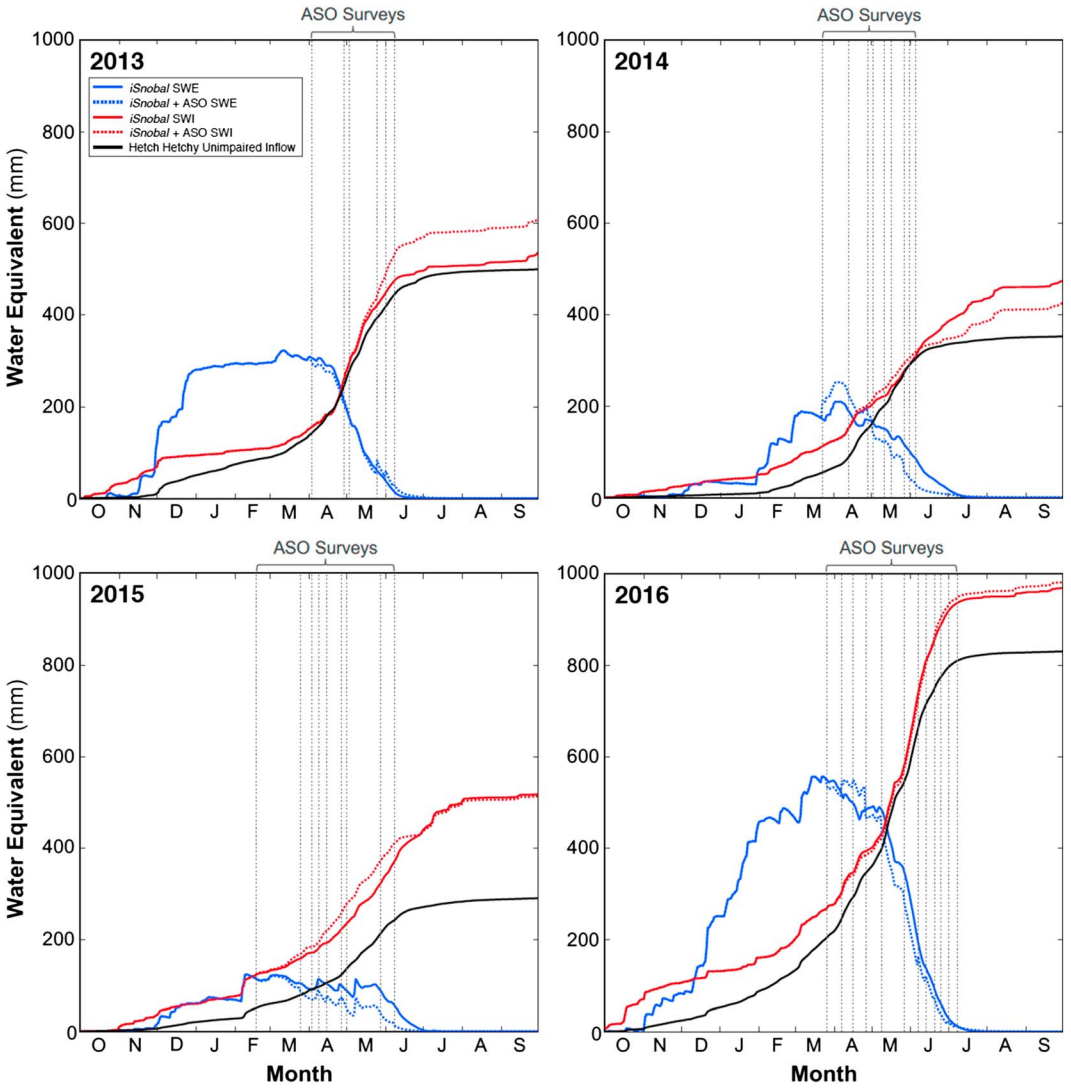

Figure 8. Basin-averaged *iSnobal* model results for both the unmodified predictions and the ASO-derived snow depth updates to the model state. The blue line is SWE and red line is the cumulative surface water input (SWI) from either the base of the snowpack or rain on bare ground. The solid black line is the estimated cumulative inflow to Hetch Hetchy Reservoir (courtesy of the San Francisco Public Utilities Commission). The dashed vertical lines represent the timing of each lidar survey used to update the model.

year 2014 in Figure 8. If a more robust DA technique that considered error in ASO snow depths was employed, the sharp increase in SWE magnitude for the first ASO update would perhaps be less abrupt.

Errors in both the lidar processing chain as well as in the model forcing data can be difficult to diagnose in near real time and are often only apparent in hindsight after subsequent updates, which is not possible within the operational ASO mission structure. In the future, for purposes of modeled SWE accuracy, a filtering mechanism will be developed to locate regions in the lidar snow depth product that depart from previous ASO surveys in ways that are not consistent with measured or modeled precipitation.

The basin-averaged SWE and cumulative SWI as a function of time for all four water years (Figure 8) reveal model shortcomings that will be addressed in future near-real-time applications. For 2013 and 2014, the cumulative SWI was altered after the inclusion of the updates. The causes for this are large abrupt changes in SWE storage during the ablation period. When ASO added SWE in updates #4 and #5 of 2013, the total amount of available meltwater was suddenly increased. In 2014, updates #3, #4, #6, and #7 decreased the SWE storage and available meltwater by a combined nearly 80 mm, which is evident in the decreased

cumulative SWI. A solution to these discrepancies could be more accurate parameterizations of the processes that influence melt, such as albedo decay rates or thermal radiation from snow-free surfaces in areas of patchy snow cover. However, getting the correct precipitation mass into the basin, as either rain or snow, would have the largest impact on cumulative SWI.

The difference between the cumulative SWI (red lines) and inflow to the Hetch Hetchy Reservoir (black line) is the residual to the hydrologic water balance of this basin, which is defined as the sum of total annual evapotranspiration (ET) and ground water losses. Henn et al. (2018) estimated ET over the ablation period in 2013, 2014, and 2015 to be 168, 161, and 191 mm, respectively, with 2016 not considered. The disagreement of those findings with the residuals in Figure 8 are likely due to precipitation inputs to *iSnobal*, causing the abrupt changes in modeled SWE described above. ASO is able to adjust the modeled SWE but not precipitation that falls as rain, which can be up to a third of the precipitation input annually.

The metrics presented in Table 3 show that many aspects of the basin hydrology were adversely affected by the severe snow drought year of 2015. During this year, far more precipitation fell as rain, the average rain-snow transition elevation was higher, and the date of peak SWE was much earlier. Such analyses of the spatial sensitivities of a snowpack are made possible with the use of a high resolution distributed snow model such as *iSnobal*. Additionally, the ASO proved to be most critical in 2015 given that the model without ASO updates was in diminished agreement. The integration of modeling and remote sensing is far more effective and powerful than either on its own.

The Tuolumne Basin hypsometry is unusual due to the steepness of the lower Tuolumne valley. Small changes in rain snow transition elevation can have large effects on snowpack water storage. The annual cumulative SWI for 2015 (Figure 8) was close to 2013 levels and actually higher than 2014 due to monsoonal rainfall in May and June, yet the peak SWE volume was one third and one half of those years, respectively. Consequently, a large contributor to the catastrophic snow drought of 2015 was the 566-m average upward shift in the rain-snow transition elevation from that of a relatively normal year of 2016 (Table 3). The second column of Table 3 shows a decrease in annual phase proportion of snowfall of approximately 12–13% in 2015 from the remaining water years and was likely a contributing factor to the historically meager snowpack. A detailed analysis of the rain-snow transition elevation in the Tuolumne Basin will be addressed in a following study.

6. Conclusions

The mountain snow cover is heterogeneously distributed across a complex landscape (Jost et al., 2007; Lehning et al., 2011) and is notoriously difficult to characterize. With ASO, the approximated and more uniform modeled snow distribution can be replaced with observations from the airborne lidar. While the total basin storage is not drastically changed by the lidar snow depths, the snow covered area, timing of melt, and the hydrologic system are affected by the redefined snow distribution. The integration of modeling and remote sensing in the ASO program provides a unique opportunity to quantify the volume of water stored in the seasonal snow cover of a large mountain basin. It can also provide a reliable definition of how that SWE is distributed across the basin and show the timing and pattern of SWI at the snow-soil interface.

Explicitly redefining the spatial snowpack distribution had a similar net effect on the available water from the basin for all four years between 2013 and 2016. Each winter the first update to the near-real-time *iSnobal* predictions using the ASO lidar-derived snow depths increased the basin averaged SWE estimates at high elevations (above 3,000 m) where wind redistribution is a major factor, while the subsequent updates throughout the melt season resulted in earlier melt out dates for elevations below 3,000 m. The time series of ASO overflights provide the first detailed definition of snow distribution and how that distribution changes throughout the snow season. Integration of these into the *iSnobal* data stream shows us that the first ASO update represents the largest adjustment because it defines the basic distribution. Subsequent updates generally involve much smaller adjustments but are equally important because they define the effect of additional deposition on the snow distribution and adjustments as snow cover depletion progresses during the snow season.

From spatiotemporal analysis of the updated *iSnobal* SWE product over the four study years, we were able to explicitly derive the average rain-snow transition on a storm-by-storm basis. In 2015, the Tuolumne Basin

experienced a reduction of almost 13% in the snow to rain precipitation ratio and a mean upward shift in rain-snow transition elevation of 566 m from the average snowpack year of 2016 (Table 3).

Future work will include perturbed forcing grids for executing ensemble *iSnobal* runs in order to better understand model uncertainty. Also, in basins with highly suspect or a complete lack of station measurements, gridded forcing data from sources such as the Modern-Era Retrospective Analysis for Research and Application (MERRA), the North American Land Data Assimilation System (NLDAS), or the High-Resolution Rapid Refresh (HRRR) forecast must be downscaled to the *iSnobal*/ASO resolution, which will require extensive validation. Likewise, total error propagation techniques are being developed by the ASO team to provide a more rigorous uncertainty estimate for the lidar-derived snow depths, the simulated SWE and SWI, and the integrated remote sensing and snow modeling result. With a better understanding of the uncertainty for both the model and the remote sensing measurements, we may move forward with an improved integration of the ASO snow depths into *iSnobal* leading to a more effective overall ASO product.

Acknowledgments

We would like to thank Aaron Fellows, Jim Roche, Ned Bair, Jeff Dozier, Jessica Lundquist, and two anonymous reviewers for their very insightful comments and suggestions. The data and analysis presented in this paper were funded in part by USDA-ARS CRIS Understanding Snow and Hydrologic Processes in Mountainous Terrain with a Changing Climate (5362-13610-008-00D), USDA-ARS Pathways Program, NASA Terrestrial Hydrology Program, NRCS Water and Climate Center, Bureau of Reclamation Pacific Northwest Region, California Department of Water Resources, and the NASA Applied Sciences Western Water Applications Office. Any reference to specific equipment types or manufacturers is for information purposes and does not represent a product endorsement or recommendation. USDA is an equal opportunity provider and employer. Part of this work was performed at the California Institute of Technology under a contract with the National Aeronautics and Space Administration. The data set used to produce the results presented in this study is available at https://doi.org/10.5281/zenodo.1343653. The interpolation from point to grid for the forcing data is available as a standalone Docker container in a software repository at https://doi.org/10.5281/zenodo.1343647.

References

Anderton, S. P., White, S. M., & Alvera, B. (2004). Evaluation of spatial variability in snow water equivalent for a high mountain catchment. *Hydrological Processes*, *18*(3), 435–453. https://doi.org/10.1002/hyp.1319

Auvinen, H., Bardsley, J. M., Haario, H., & Kauranne, T. (2010). The variational Kalman filter and an efficient implementation using limited memory BFGS. *International Journal for Numerical Methods in Fluids*, *64*(3), 314–335. https://doi.org/10.1002/fld.2153

Bair, E. H., Davis, R. E., & Dozier, J. (2018). Hourly mass and snow energy balance measurements from Mammoth Mountain, CA USA, 2011–2017. *Earth System Science Data*, *10*(1), 549–563. https://doi.org/10.5194/essd-10-549-2018

Belmecheri, S., Babst, F., Wahl, E. R., Stahle, D. W., & Trouet, V. (2016). Multi-century evaluation of Sierra Nevada snowpack. *Nature Climate Change*, *6*(1), 2–3. https://doi.org/10.1038/nclimate2809

Brauchli, T., Trujillo, E., Huwald, H., & Lehning, M. (2017). Influence of slope-scale snowmelt on catchment response simulated with the Alpine3D model. *Water Resources Research*, *53*, 10,723–10,739. https://doi.org/10.1002/2017WR021278

Conway, H., & Abrahamson, J. (1984). Snow stability index. *Journal of Glaciology*, *30*(106), 321–327. https://doi.org/10.1017/S002214300000616X

Deems, J. S., Fassnacht, S. R., & Elder, K. J. (2006). Fractal distribution of snow depth from lidar data. *Journal of Hydrometeorology*, *7*(2), 285–297. https://doi.org/10.1175/JHM487.1

Deems, J. S., & Painter, T. H. (2006). Lidar measurement of snow depth: accuracy and error sources. In *Proceedings, 2006 International Snow Science Workshop, Telluride, CO* (Vol. 330, pp. 330–338). Telluride, CO.

Deems, J. S., Painter, T. H., & Finnegan, D. C. (2013). Lidar measurement of snow depth: A review. *Journal of Glaciology*, *59*(215), 467–479. https://doi.org/10.3189/2013JoG12J154

Derksen, C., & Brown, R. (2012). Spring snow cover extent reductions in the 2008-2012 period exceeding climate model projections. *Geophysical Research Letters*, *39*, L19504. https://doi.org/10.1029/2012GL053387

Dettinger, M. D., & Anderson, M. L. (2015). Storage in California's reservois and snowpack in this time of drought. *San Francisco Estuary and Watershed Science*, *13*(2), 0–5. https://doi.org/10.15447/sfews.2015v13iss2art1

Dozier, J. (1980). A clear-sky spectral solar radiation model for snow-covered mountainous terrain. *Water Resources Research*, *16*(4), 709–718. https://doi.org/10.1029/WR016i004p00709

Dozier, J. (1990). Looking ahead to EOS: The Earth Observing System. *Computers in Physics*, *4*(3), 248–259. https://doi.org/10.1063/1.4822913

Dozier, J. (2011). Mountain hydrology, snow color, and the fourth paradigm. *Eos, Transactions American Geophysical Union*, *92*(43), 373–374. https://doi.org/10.1029/2011EO430001

Essery, R., & Marks, D. (2007). Scaling and parametrization of clear-sky solar radiation over complex topography. *Journal of Geophysical Research*, *112*, D10122. https://doi.org/10.1029/2006JD007650

Essery, R., & Pomeroy, J. (2004). Implications of spatial distributions of snow mass and melt rate for snow-cover depletion: Theoretical considerations. *Annals of Glaciology*, *38*(1), 261–265. https://doi.org/10.3189/172756404781815275

Essery, R., Pomeroy, J., Ellis, C., & Link, T. (2008). Modelling longwave radiation to snow beneath forest canopies using hemispherical photography or linear regression. *Hydrological Processes*, *22*(15), 2788–2800. https://doi.org/10.1002/hyp.6930

Garen, D. C., Geyer, J., Schumann, A. H., & Marks, D. (2001). Spatially-distributed snowmelt, water balance and streamflow modelling for a large mountainous catchment: Boise River, Idaho, USA. In *Soil-vegetation-atmosphere transfer schemes and large-scale hydrological models* (Vol. 270, pp. 199–207). Maastricht, The Netherlands: Sixth IAHS Scientific Assembly.

Garen, D. C., Johnson, G. L., & Hanson, C. L. (1994). Mean areal precipitation for daily hydrologic modeling in mountainous regions. *JAWRA Journal of the American Water Resources Association*, *30*(3), 481–491. https://doi.org/10.1111/j.1752-1688.1994.tb03307.x

Garen, D. C., & Marks, D. (2005). Spatially distributed energy balance snowmelt modelling in a mountainous river basin: Estimation of meteorological inputs and verification of model results. *Journal of Hydrology*, *315*(1–4), 126–153. https://doi.org/10.1016/j.jhydrol.2005.03.026

Goovaerts, P. (2000). Geostatistical approaches for incorporating elevation into the spatial interpolation of rainfall. *Journal of Hydrology*, *228*(1–2), 113–129. https://doi.org/10.1016/S0022-1694(00)00144-X

Griffin, D., & Anchukaitis, K. J. (2014). How unusual is the 2012–2014 California drought? *Geophysical Research Letters*, *41*, 9017–9023. https://doi.org/10.1002/2014GL062433

Grünewald, T., Schirmer, M., Mott, R., & Lehning, M. (2010). Spatial and temporal variability of snow depth and ablation rates in a small mountain catchment. *The Cryosphere*, *4*(2), 215–225. https://doi.org/10.5194/tc-4-215-2010

Guan, B., Molotch, N. P., Waliser, D. E., Jepsen, S. M., Painter, T. H., & Dozier, J. (2013). Snow water equivalent in the Sierra Nevada: Blending snow sensor observations with snowmelt model simulations. *Water Resources Research*, *49*, 5029–5046. https://doi.org/10.1002/wrcr.20387

Hardy, J., Melloh, R., Koenig, G., Marks, D., Winstral, A., Pomeroy, J., & Link, T. (2004). Solar radiation transmission through conifer canopies. *Agricultural and Forest Meteorology*, *126*(3–4), 257–270. https://doi.org/10.1016/j.agrformet.2004.06.012

Havens, S., Marks, D., Kormos, P., & Hedrick, A. (2017). Spatial Modeling for Resources Framework (SMRF): A modular framework for developing spatial forcing data for snow modeling in mountain basins. *Computers and Geosciences*, *109*(September 2016), 295–304. https://doi.org/10.1016/j.cageo.2017.08.016

Havens, S., Marks, D., & Rothwell, E. (2016). Application of a physically-based distributed snowmelt model in support of reservoir operations and water management—Phase 2. Retrieved from https://www.usbr.gov/research/projects/detail.cfm?id=2157

Hedrick, A. R., Marks, D., Havens, S., Robertson, M., Johnson, M., Sandusky, M., et al. (2018a). Direct insertion of NASA Airborne Snow Observatory-derived snow depth time-series into the iSnobal energy balance snow model [Data set]. Zenodo. https://doi.org/10.5281/zenodo.1343653

Hedrick, A. R., Marks, D., Havens, S., Robertson, M., Johnson, M., Sandusky, M., et al. (2018b). Direct insertion of NASA Airborne Snow Observatory-derived snow depth time-series into the iSnobal energy balance snow model [Software version 0.1]. Zenodo. https://doi.org/10.5281/zenodo.1343647

Henn, B., Painter, T. H., Bormann, K. J., McGurk, B., Flint, A. L., Flint, L. E., et al. (2018). High-elevation evapotranspiration estimates during drought: Using streamflow and NASA airborne snow observatory SWE observations to close the upper Tuolumne River Basin water balance. *Water Resources Research*, *54*, 746–766. https://doi.org/10.1002/2017WR020473

Horel, J., Splitt, M., Dunn, L., Pechmann, J., White, B., Ciliberti, C., et al. (2002). Mesowest: Cooperative Mesonets in the western United States. *Bulletin of the American Meteorological Society*, *83*(2), 211–225. https://doi.org/10.1175/1520-0477(2002)083<0211:MCMITW>2.3.CO;2

Houser, P. R., De Lannoy, G. J. M., & Walker, J. P. (2012). Hydrologic data assimilation. In Approaches to managing disaster—Assessing hazards, emergencies and disaster impacts. *INTECH*, 41–64. https://doi.org/10.5772/31246

Jost, G., Weiler, M., Gluns, D. R., & Alila, Y. (2007). The influence of forest and topography on snow accumulation and melt at the watershed-scale. *Journal of Hydrology*, *347*(1–2), 101–115. https://doi.org/10.1016/j.jhydrol.2007.09.006

Kojima, K. (1967). Densification of seasonal snow cover. *Low Temperature Science*, *799*, 929–952.

Kormos, P., Marks, D., McNamara, J. P., Marshall, H.-P., Winstral, A. H., & Flores, A. N. (2014). Snow distribution, melt and surface water inputs to the soil in the mountain rain–snow transition zone. *Journal of Hydrology*, *519*, 190–204. https://doi.org/10.1016/j.jhydrol.2014.06.051

Lehning, M., Grünewald, T., & Schirmer, M. (2011). Mountain snow distribution governed by an altitudinal gradient and terrain roughness. *Geophysical Research Letters*, *38*, L19504. https://doi.org/10.1029/2011GL048927

Link, T. E., & Marks, D. (1999). Point simulation of seasonal snow cover dynamics beneath boreal forest canopies. *Journal of Geophysical Research*, *104*(D22), 27,827–841,857. https://doi.org/10.1029/1998JD200121

Link, T. E., Marks, D., & Hardy, J. P. (2004). A deterministic method to characterize canopy radiative transfer properties. *Hydrological Processes*, *18*(18), 3583–3594. https://doi.org/10.1002/hyp.5793

Livneh, B., Deems, J. S., Schneider, D., Barsugli, J. J., & Molotch, N. P. (2014). Filling in the gaps: Inferring spatially distributed precipitation from gauge observations over complex terrain. *Water Resources Research*, *50*, 8589–8610. https://doi.org/10.1002/2014WR015442

Luce, C. H., Tarboton, D. G., & Cooley, K. R. (1999). Sub-grid parameterization of snow distribution for an energy and mass balance snow cover model. *Hydrological Processes*, *13*(12–13), 1921–1933. https://doi.org/10.1002/(SICI)1099-1085(199909)13:12/13<1921::AID-HYP867>3.0.CO;2-S

Lundquist, J. D., Minder, J. R., Neiman, P. J., & Sukovich, E. (2010). Relationships between barrier jet heights, orographic precipitation gradients, and streamflow in the Northern Sierra Nevada. *Journal of Hydrometeorology*, *11*(5), 1141–1156. https://doi.org/10.1175/2010JHM1264.1

Lundquist, J. D., Roche, J. W., Forrester, H., Moore, C., Keenan, E., Perry, G., et al. (2016). Yosemite Hydroclimate Network: Distributed stream and atmospheric data for the Tuolumne River watershed and surroundings. *Water Resources Research*, *52*, 7478–7489. https://doi.org/10.1002/2016WR019261

Luo, W., Taylor, M. C., & Parker, S. R. (2008). A comparison of spatial interpolation methods to estimate continuous wind speed surfaces using irregularly distributed data from England and Wales. *International Journal of Climatology*, *28*(7), 947–959. https://doi.org/10.1002/joc.1583

Margulis, S. A., Cortés, G., Girotto, M., Huning, L. S., Li, D., & Durand, M. (2016). Characterizing the extreme 2015 snowpack deficit in the Sierra Nevada (USA) and the implications for drought recovery. *Geophysical Research Letters*, *43*, 6341–6349. https://doi.org/10.1002/2016GL068520

Marks, D., Domingo, J., Susong, D., Link, T. E., & Garen, D. C. (1999). A spatially distributed energy balance snowmelt model for application in mountain basins. *Hydrological Processes*, *13*(12–13), 1935–1959. https://doi.org/10.1002/(SICI)1099-1085(199909)13:12/13<1935::AID-HYP868>3.0.CO;2-C

Marks, D., & Dozier, J. (1979). A clear-sky longwave radiation model for remote alpine areas. *Archiv Für Meteorologie, Geophysik Und Bioklimatologie Serie B*, *27*(2–3), 159–187. https://doi.org/10.1007/BF02243741

Marks, D., & Dozier, J. (1992). Climate and energy exchange at the snow surface in the Alpine Region of the Sierra Nevada: 2. Snow cover energy balance. *Water Resources Research*, *28*(11), 3043–3054. https://doi.org/10.1029/92WR01483

Marshall, S. E., & Warren, S. G. (1987). Parameterization of snow albedo for climate models. In B. E. Goodison, R. G. Barry, & J. Dozier (Eds.), *Large scale effects of seasonal snow cover* (pp. 43–50). Wallingford, England: International Association of Hydrological Sciences.

Miller, R. N., Ghil, M., & Gauthiez, F. (1994). Advanced data assimilation in strongly nonlinear dynamical systems. *Journal of the Atmospheric Sciences*, *51*(8), 1037–1056. https://doi.org/10.1175/1520-0469(1994)051<1037:ADAISN>2.0.CO;2

Molotch, N. P., & Bales, R. C. (2005). Scaling snow observations from the point to the grid element: Implications for observation network design. *Water Resources Research*, *41*, W11421. https://doi.org/10.1029/2005WR004229

Molotch, N. P., Painter, T. H., Bales, R. C., & Dozier, J. (2004). Incorporating remotely-sensed snow albedo into a spatially-distributed snowmelt model. *Geophysical Research Letters*, *31*, L03501. https://doi.org/10.1029/2003GL019063

Nayak, A., Chandler, D. G., Marks, D., McNamara, J. P., & Seyfried, M. S. (2008). Correction of electronic record for weighing bucket precipitation gauge measurements. *Water Resources Research*, *44*, W00D11. https://doi.org/10.1029/2008WR006875

Olyphant, G. A., & Isard, S. A. (1988). The role of advection in the energy balance of late-lying snowfields: Niwot Ridge, Front Range, Colorado. *Water Resources Research*, *24*(11), 1962–1968. https://doi.org/10.1029/WR024i011p01962

Painter, T. H., Berisford, D. F., Boardman, J. W., Bormann, K. J., Deems, J. S., Gehrke, F., et al. (2016). The Airborne Snow Observatory: Fusion of scanning lidar, imaging spectrometer, and physically-based modeling for mapping snow water equivalent and snow albedo. *Remote Sensing of Environment*, *184*, 139–152. https://doi.org/10.1016/j.rse.2016.06.018

Pomeroy, J., Bewley, D. S., Essery, R., Hedstrom, N. R., Link, T., Granger, R., et al. (2006). Shrub tundra snowmelt. *Hydrological Processes*, *20*(4), 923–941. https://doi.org/10.1002/hyp.6124

Pomeroy, J., & Brun, E. (2001). Physical properties of snow. In H. G. Jones, J. W. Pomeroy, D. A. Walker, & R. W. Hoham (Eds.), *Snow ecology: An interdisciplinary examination of snow-covered ecosystems* (pp. 45–126). Cambridge: Cambridge University Press.

Prokop, A. (2008). Assessing the applicability of terrestrial laser scanning for spatial snow depth measurements. *Cold Regions Science and Technology*, *54*(3), 155–163. https://doi.org/10.1016/j.coldregions.2008.07.002

Rasmussen, R., Baker, B., Kochendorfer, J., Meyers, T., Landolt, S., Fischer, A. P., et al. (2012). How well are we measuring snow: The NOAA/FAA/NCAR winter precipitation test bed. *Bulletin of the American Meteorological Society*, *93*(6), 811–829. https://doi.org/10.1175/BAMS-D-11-00052.1

Reba, M. L., Marks, D., Seyfried, M. S., Winstral, A. H., Kumar, M., & Flerchinger, G. N. (2011). A long-term data set for hydrologic modeling in a snow-dominated mountain catchment. *Water Resources Research*, *47*, W07702. https://doi.org/10.1029/2010WR010030

Shook, K., & Gray, D. M. (1996). Small-scale spatial structure of shallow snowcovers. *Hydrological Processes*, *10*(10), 1283–1292. https://doi.org/10.1002/(SICI)1099-1085(199610)10:10<1283::AID-HYP460>3.0.CO;2-M

Sturm, M., Taras, B., Liston, G. E., Derksen, C., Jonas, T., & Lea, J. (2010). Estimating snow water equivalent using snow depth data and climate classes. *Journal of Hydrometeorology*, *11*(6), 1380–1394. https://doi.org/10.1175/2010JHM1202.1

Susong, D., Marks, D., & Garen, D. (1999). Methods for developing time-series climate surfaces to drive topographically distributed energy- and water-balance models. *Hydrological Processes*, *13*(12–13), 2003–2021. https://doi.org/10.1002/(SICI)1099-1085(199909)13:12/13<2003::AID-HYP884>3.0.CO;2-K

Tinkham, W. T., Smith, A. M. S., Marshall, H. P., Link, T. E., Falkowski, M. J., & Winstral, A. H. (2014). Quantifying spatial distribution of snow depth errors from LiDAR using Random Forest. *Remote Sensing of Environment*, *141*, 105–115. https://doi.org/10.1016/j.rse.2013.10.021

Trujillo, E., Ramírez, J. A., & Elder, K. J. (2007). Topographic, meteorologic, and canopy controls on the scaling characteristics of the spatial distribution of snow depth fields. *Water Resources Research*, *43*, W07409. https://doi.org/10.1029/2006WR005317

Vano, J. A., Das, T., & Lettenmaier, D. P. (2012). Hydrologic sensitivities of Colorado River runoff to changes in precipitation and temperature*. *Journal of Hydrometeorology*, *13*(3), 932–949. https://doi.org/10.1175/JHM-D-11-069.1

Vaughan, D. G., Comiso, J. C., Allison, I., Carrasco, J., Kaser, G., Kwok, R., et al. (2013). Observations: Cryosphere. In T. F. Stocker, et al. (Eds.), *Climate change 2013: The physical science basis, Contribution of Working Group I to the Fifth Assessment Report of the Intergovernmental Panel on Climate Change* (pp. 317–382). Cambridge, UK and New York, NY, USA: Cambridge University Press.

Vögeli, C., Lehning, M., Wever, N., & Bavay, M. (2016). Scaling precipitation input to spatially distributed hydrological models by measured snow distribution. *Frontiers in Earth Science*, *4*(December), 1–15. https://doi.org/10.3389/feart.2016.00108

Wilson, T. S., Sleeter, B. M., & Cameron, D. R. (2016). Future land-use related water demand in California. *Environmental Research Letters*, *11*(5). https://doi.org/10.1088/1748-9326/11/5/054018

Winstral, A., Elder, K., & Davis, R. E. (2002). Spatial snow modeling of wind-redistributed snow using terrain-based parameters. *Journal of Hydrometeorology*, *3*(5), 524–538. https://doi.org/10.1175/1525-7541(2002)003<0524:SSMOWR>2.0.CO;2

Winstral, A., & Marks, D. (2014). Long-term snow distribution observations in a mountain catchment: Assessing variability, time stability, and the representativeness of an index site. *Water Resources Research*, *50*, 293–305. https://doi.org/10.1002/2012WR013038

Winstral, A., Marks, D., & Gurney, R. (2009). An efficient method for distributing wind speeds over heterogeneous terrain. *Hydrological Processes*, *23*(17), 2526–2535. https://doi.org/10.1002/hyp.7141

Yang, D., Goodison, B. E., Metcalfe, J. R., Golubev, V. S., Bates, R., Pangburn, T., & Hanson, C. L. (1998). Accuracy of NWS 8 standard nonrecording precipitation gauge: Results and application of WMO Intercomparison. *Journal of Atmospheric and Oceanic Technology*, *15*(1), 54–68. https://doi.org/10.1175/1520-0426(1998)015<0054:AONSNP>2.0.CO;2